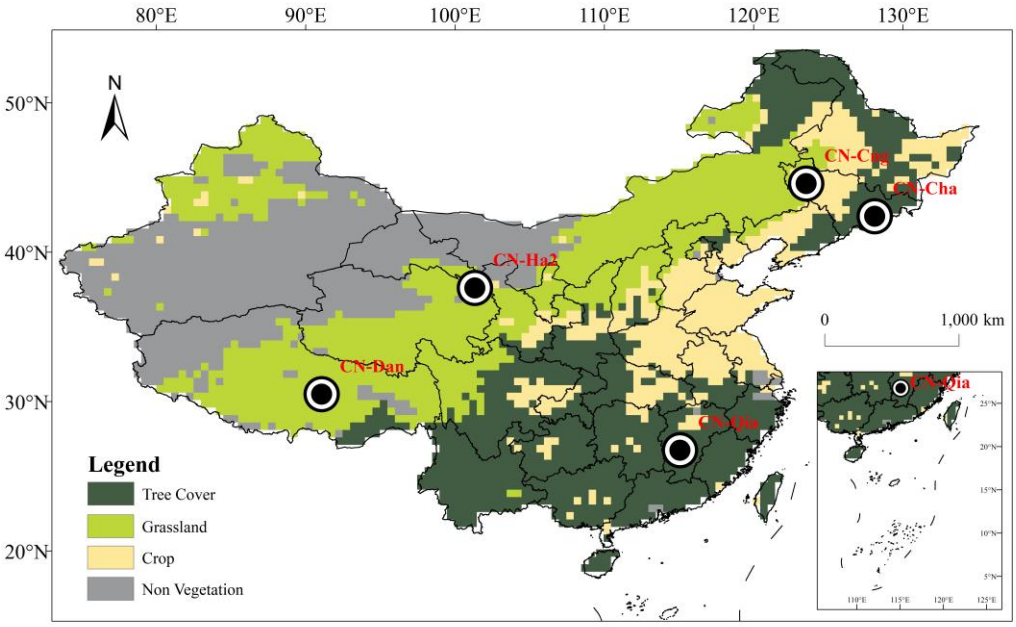

Figure S1. Regional land use classification and distribution of FLUXNET sites in China.

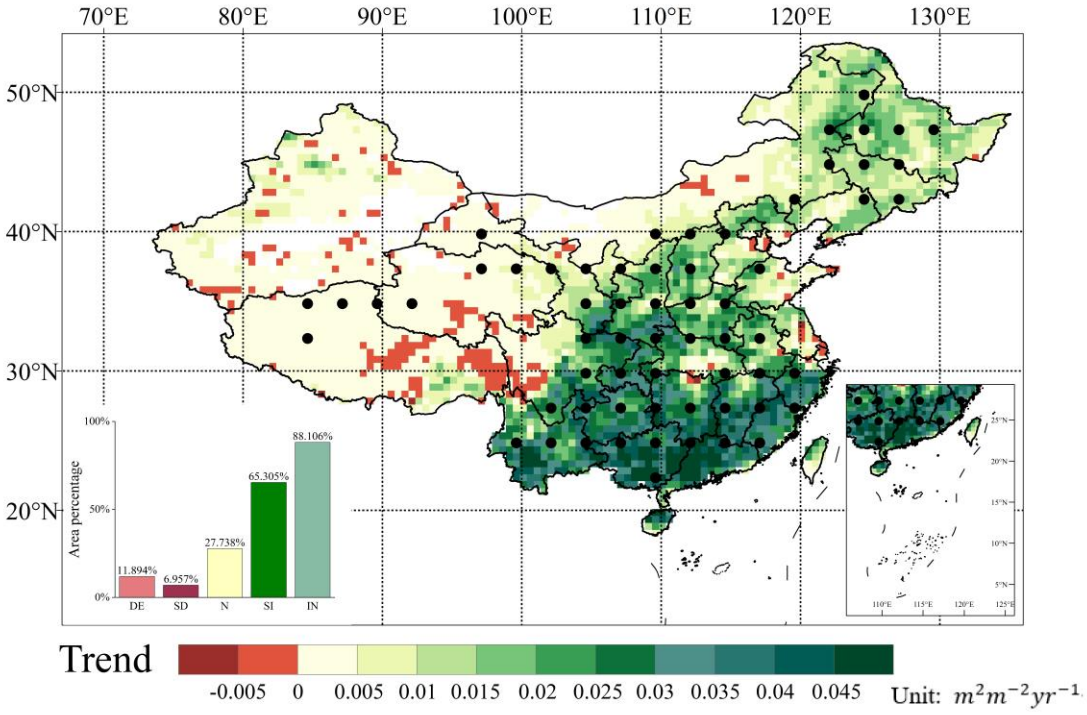

Figure S2. The observed annual MODIS LAI trend during 2003-2019 in China. Pink color represents the percentage of area of decreasing regions (DE), red color represents the percentage of area of significantly decreasing regions (SD), yellow color represents the percentage of area of regions with no significant change (N), green color represents the percentage of area of significantly increasing regions (SI), and light green color represents the percentage of area of increasing regions (IN). The dot indicated the significant trend ($p<0.05$).

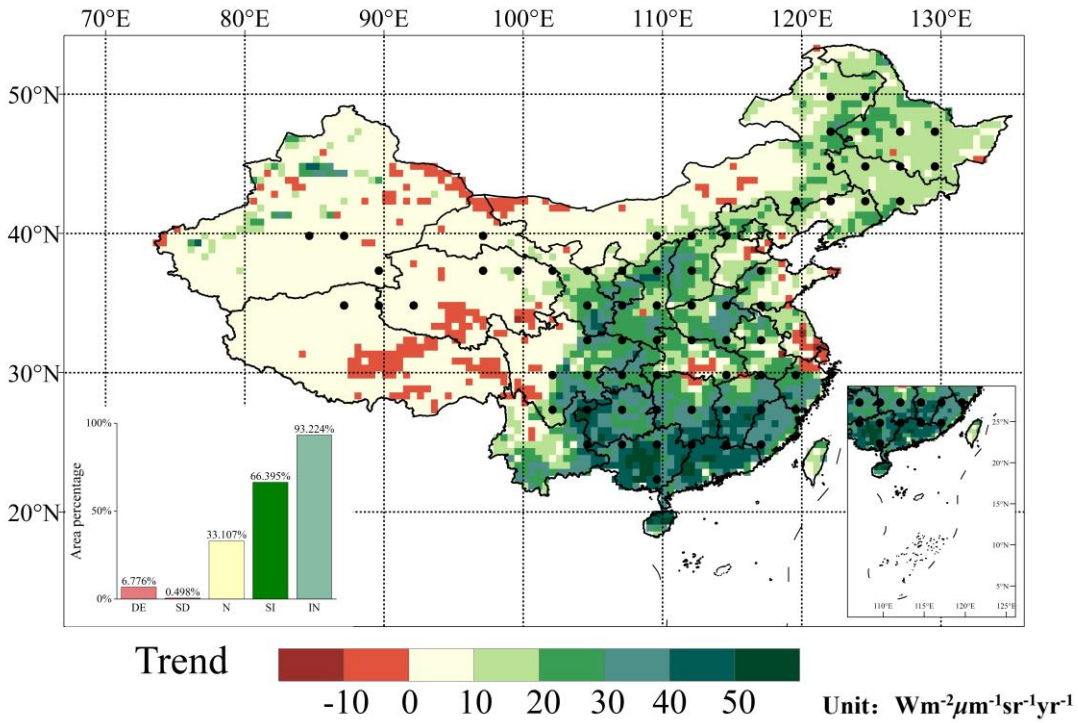

Figure S3. The observed annual CSIF trend during 2003-2019 in China. Pink color represents the percentage of area of decreasing regions (DE), red color represents the percentage of area of significantly decreasing regions (SD), yellow color represents the percentage of area of regions with no significant change (N), green color represents the percentage of area of significantly increasing regions (SI), and light green color represents the percentage of area of increasing regions (IN). The dot indicated the significant trend ($p<0.05$).

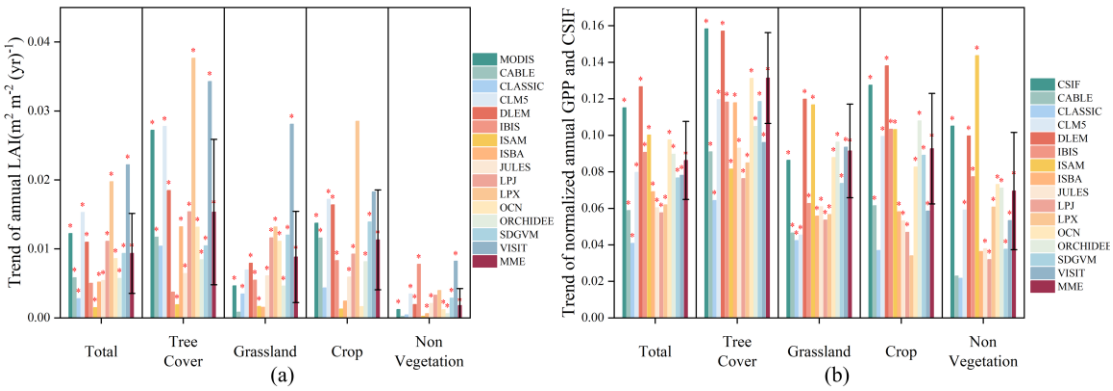

Figure S4. Overall annual average LAI and GPP trends in China during 2003-2019 over different land use types. (a) Annual trends in observed and simulated LAI; (b) Annual trends in observed and simulated GPP. The asterisk (*) indicated the significant trend ($p<0.05$).

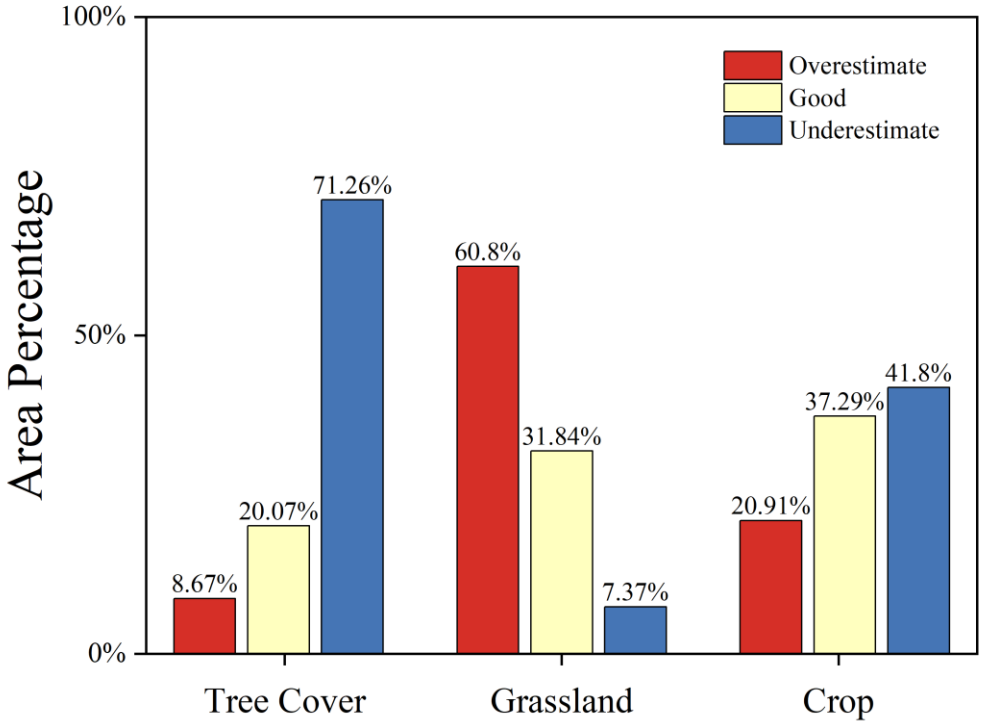

Figure S5. Percentage of simulated area misestimated by the MME for forested land, grassland, and crop.

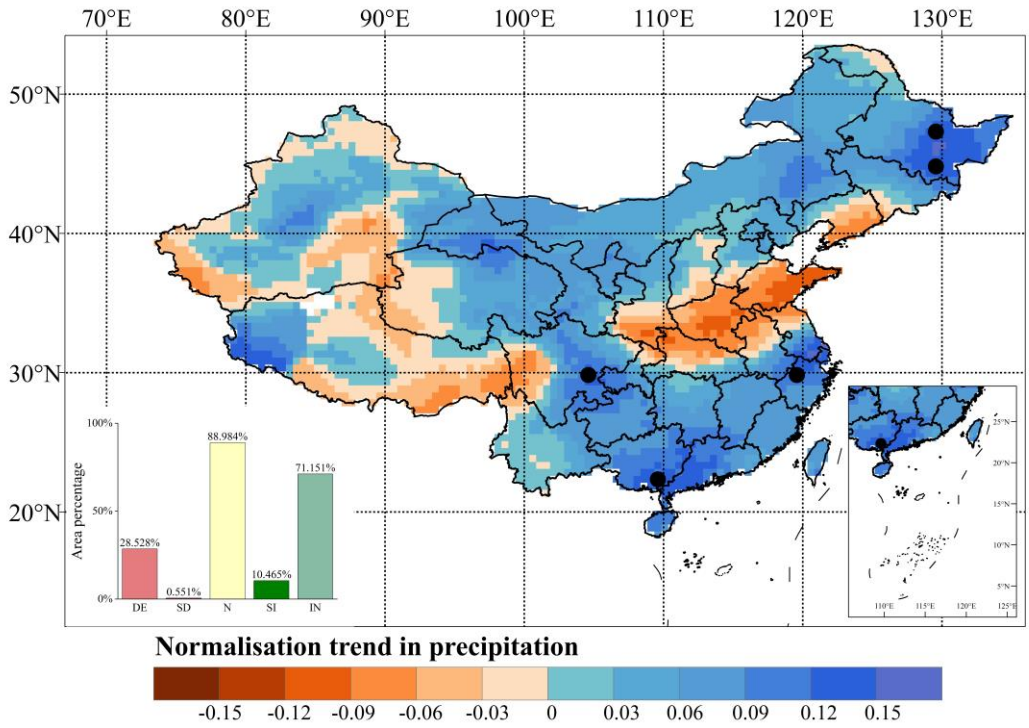

Figure S6. The observed annual spatial precipitation trend during 2003-2019 in China. Pink color represents the percentage of area in declining regions (DE), red color represents the percentage of area in significantly declining regions (SD), yellow color represents the percentage of area in regions with no significant change (N), green color represents the percentage of area in significantly increasing regions (SI), and light green color represents the percentage of area in increasing regions (IN). The dot indicated the significant trend ($p<0.05$).

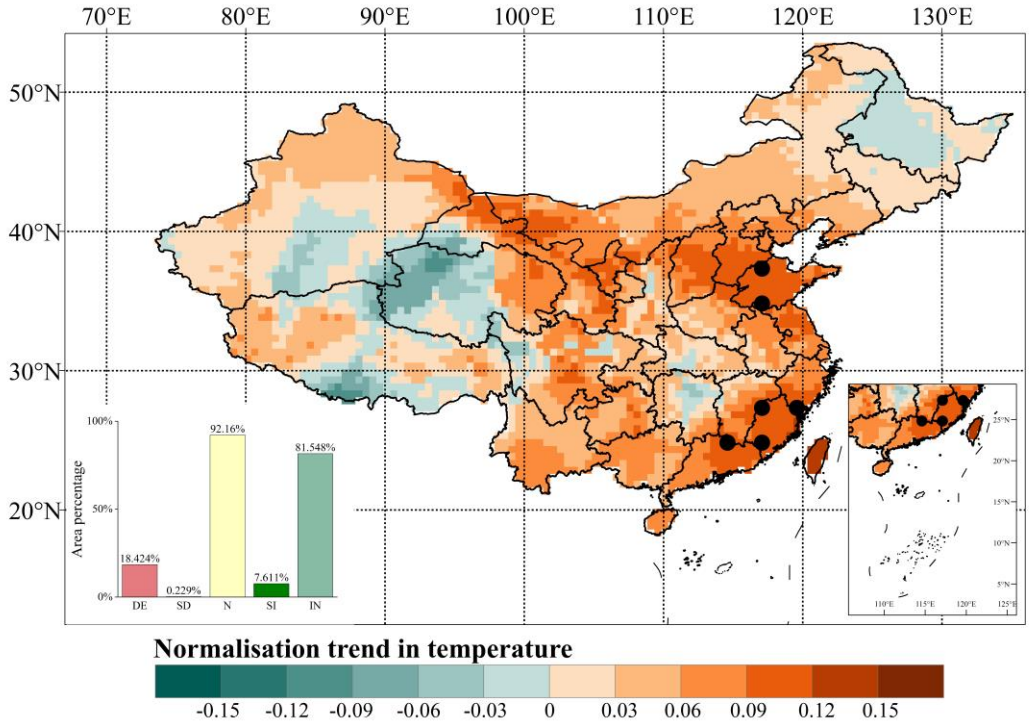

Figure S7. The observed annual spatial temperature trend during 2003-2019 in China. Pink color represents the percentage of area in declining regions (DE), red color represents the percentage of area in significantly declining regions (SD), yellow color represents the percentage of area in regions with no significant change (N), green color represents the percentage of area in significantly increasing regions (SI), and light green color represents the percentage of area in increasing regions (IN). The dot indicated the significant trend ($p<0.05$).

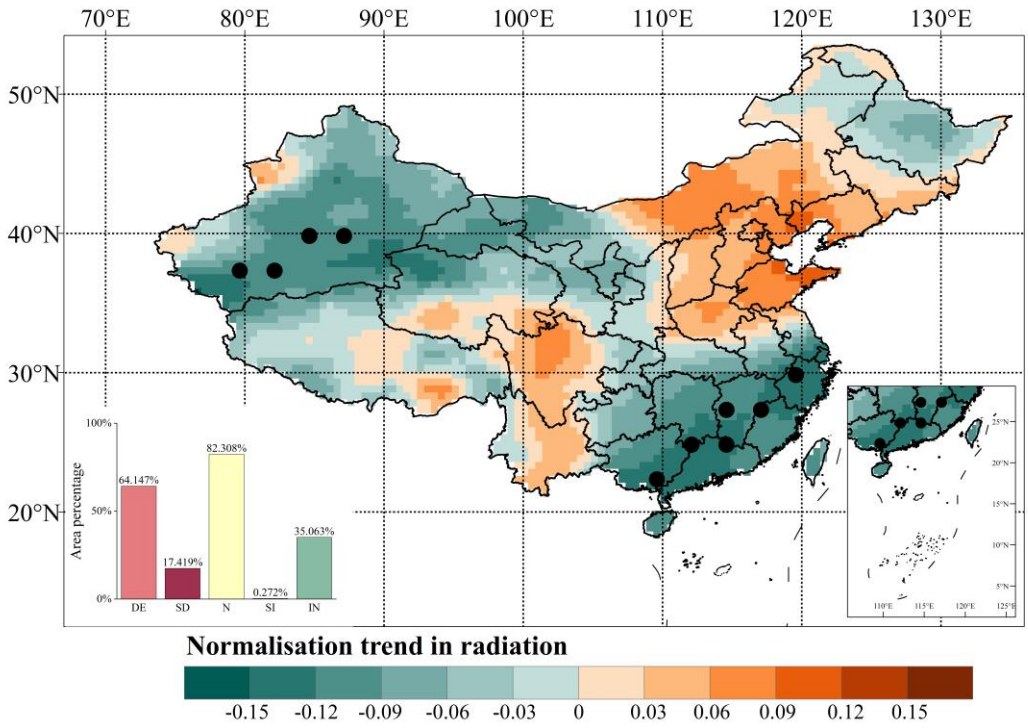

Figure S8. The observed annual spatial radiation trend during 2003-2019 in China. Pink color represents the percentage of area in declining regions (DE), red color represents the percentage of area in significantly declining regions (SD), yellow color represents the percentage of area in regions with no significant change (N), green color represents the percentage of area in significantly increasing regions (SI), and light green color represents the percentage of area in increasing regions (IN). The dot indicated the significant trend ($p<0.05$).

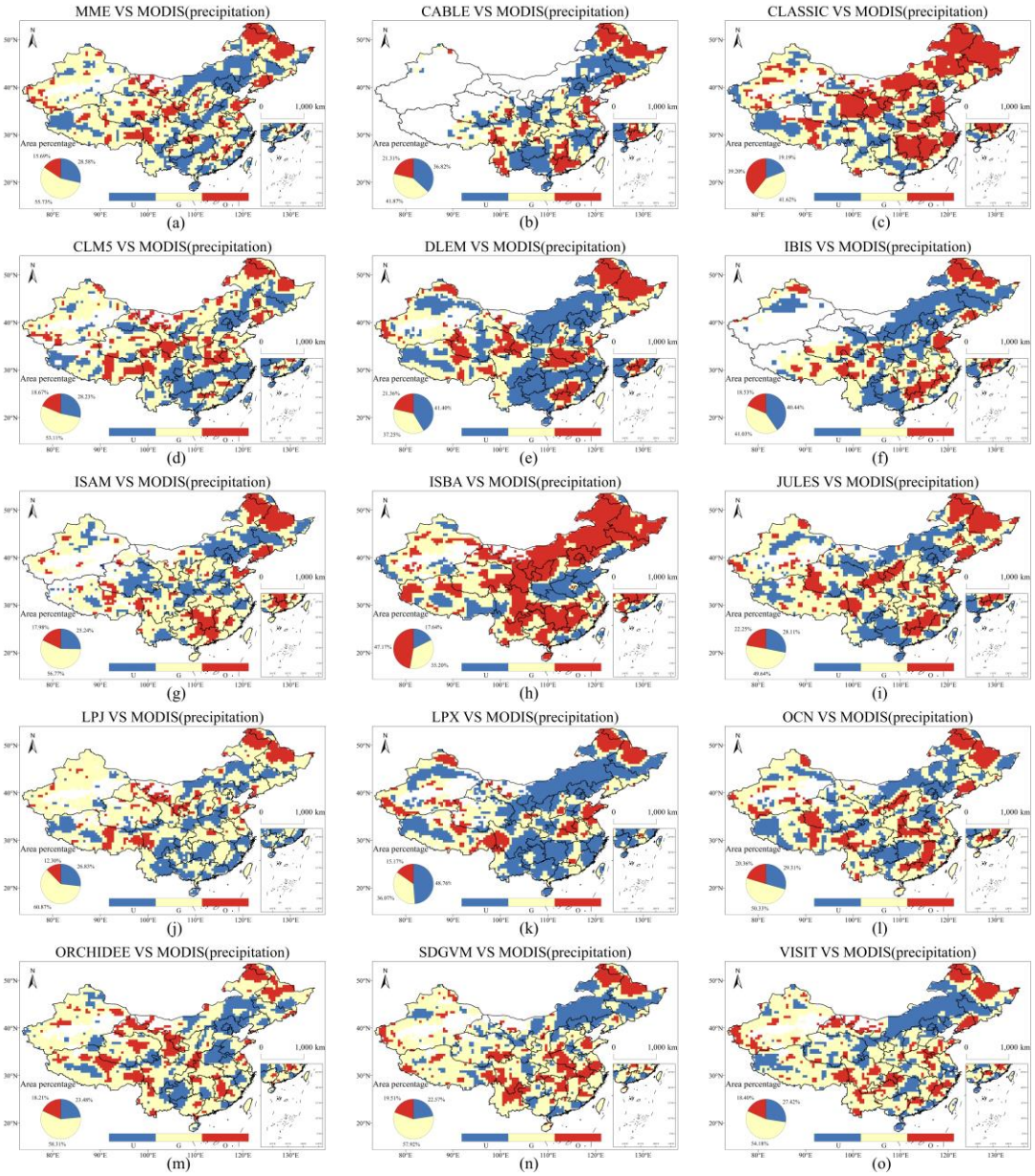

Figure S9. Spatial distribution of sensitivity differences between the effects of precipitation on observed and simulated LAI in China. A paired t-tests with a sample size of 9 were conducted using a 3 × 3 sliding window to determine whether the effect of precipitation on the amount of simulated LAI change was not significantly different from the effect on the amount of observed LAI change (Good), was significantly smaller than the observed data (Underestimate), or was significantly larger than the observed data (Overestimate).U, G, and O represent 'Underestimate', 'Good', and 'Overestimate', respectively.

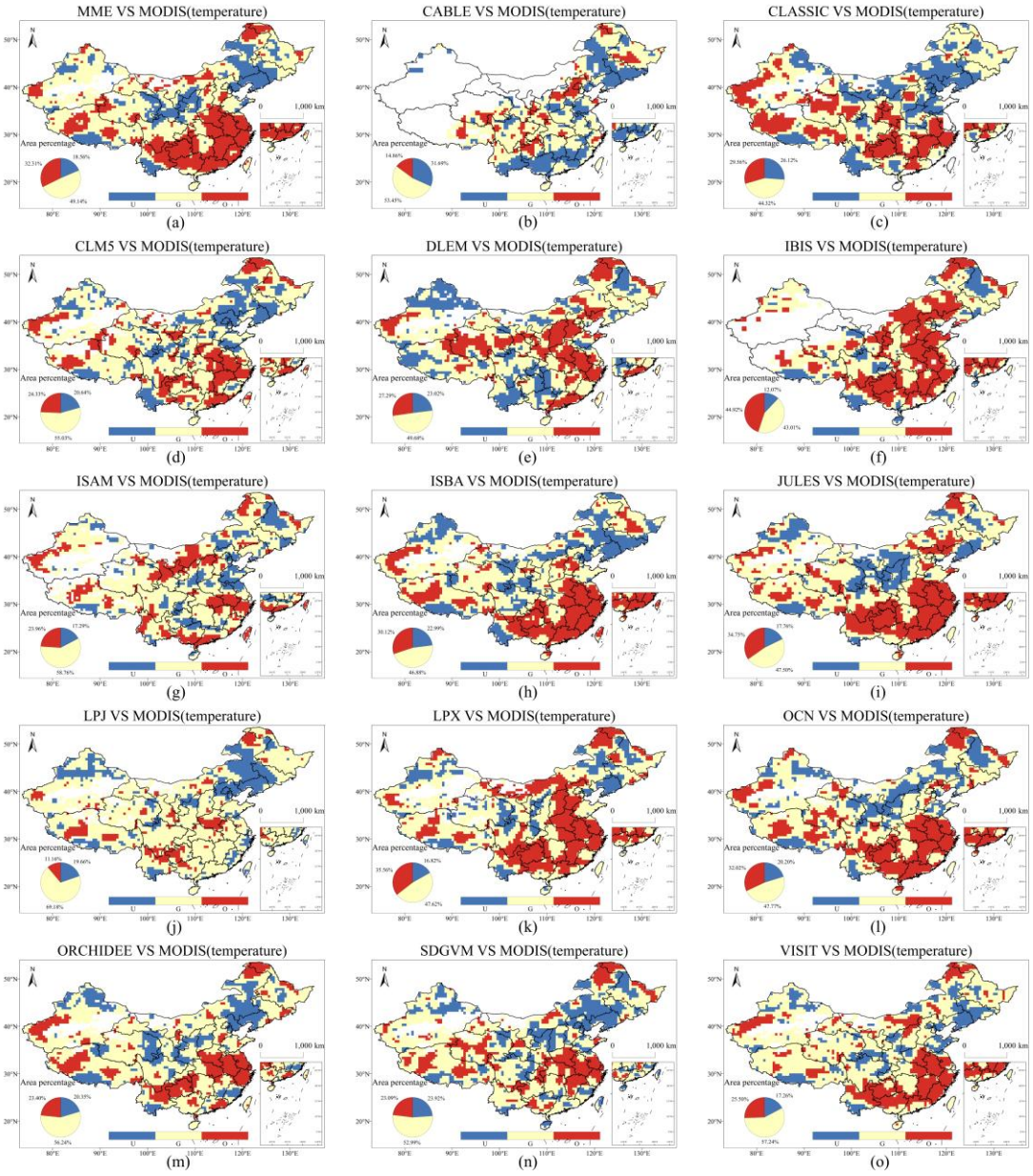

Figure S10. Spatial distribution of sensitivity differences between the effects of temperature on observed and simulated LAI in China. A paired t-tests with a sample size of 9 were conducted using a 3 × 3 sliding window to determine whether the effect of temperature on the amount of simulated LAI change was not significantly different from the effect on the amount of observed LAI change (Good), was significantly smaller than the observed data (Underestimate), or was significantly larger than the observed data (Overestimate).U, G, and O represent 'Underestimate', 'Good', and 'Overestimate', respectively.

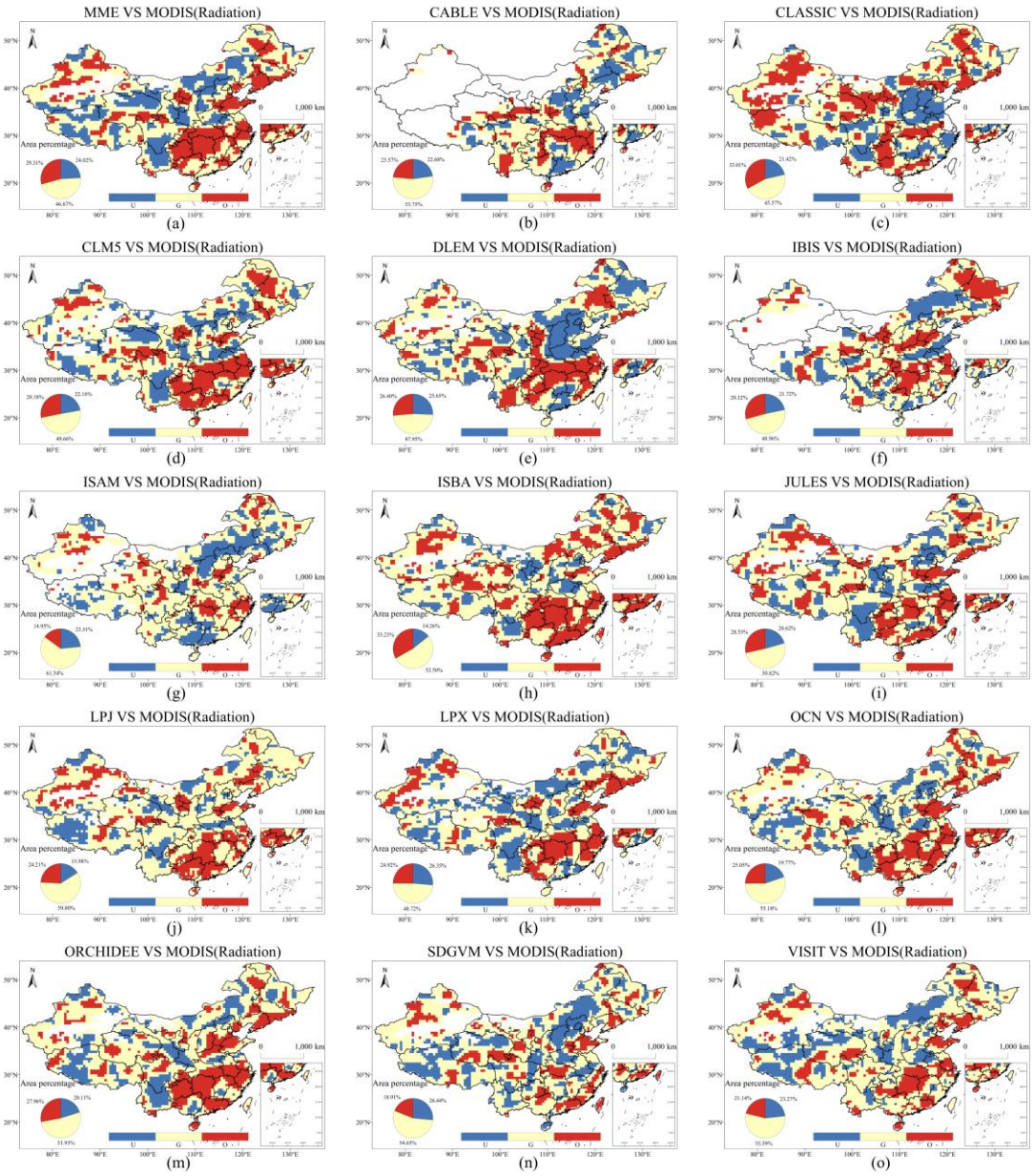

Figure S11. Spatial distribution of sensitivity differences between the effects of radiation on observed and simulated LAI in China. A paired t-tests with a sample size of 9 were conducted using a 3 × 3 sliding window to determine whether the effect of radiation on the amount of simulated LAI change was not significantly different from the effect on the amount of observed LAI change (Good), was significantly smaller than the observed data (Underestimate), or was significantly larger than the observed data (Overestimate).U, G, and O represent 'Underestimate', 'Good', and 'Overestimate', respectively.

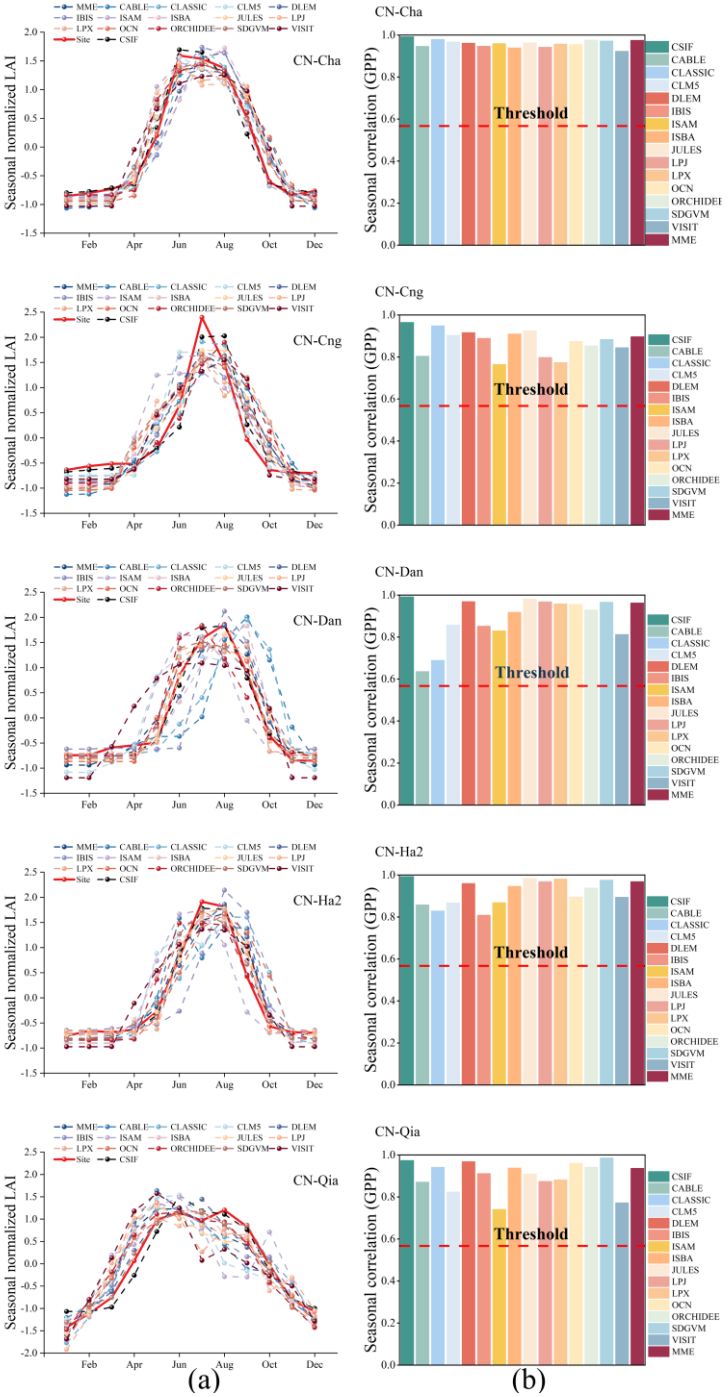

Figure S12. Seasonal performance of observed and simulated GPP in five FLUXNET sites in China. (a) The seasonal normalized GPP changes for observed and simulated GPP; (b) The seasonal correlation between the sites observed GPP and simulated GPP. The red line indicates the correlation coefficient corresponding to the significance level (p = 0.05). The values over the red line indicated that the model can capture the seasonality of CSIF in phase.

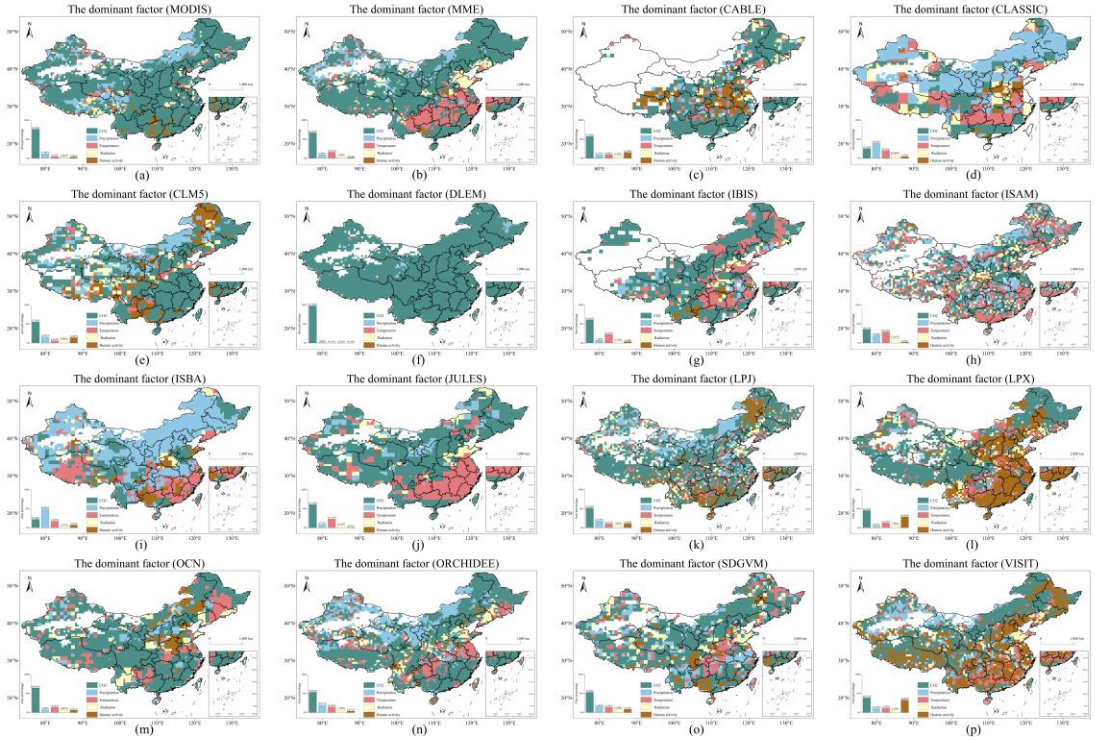

Figure S13. Spatial distribution of the dominant factors that the response of observed and simulated LAI trends to environmental and anthropogenic in China. (a) Distribution of the dominant factors in MODIS LAI trend. (b-p) Distributions of the dominant factors in MME and models LAI trend. Green, blue, red, yellow, and brown represent image elements where CO_2 concentration, precipitation, temperature, light radiation, and human activities are dominant factors, respectively.

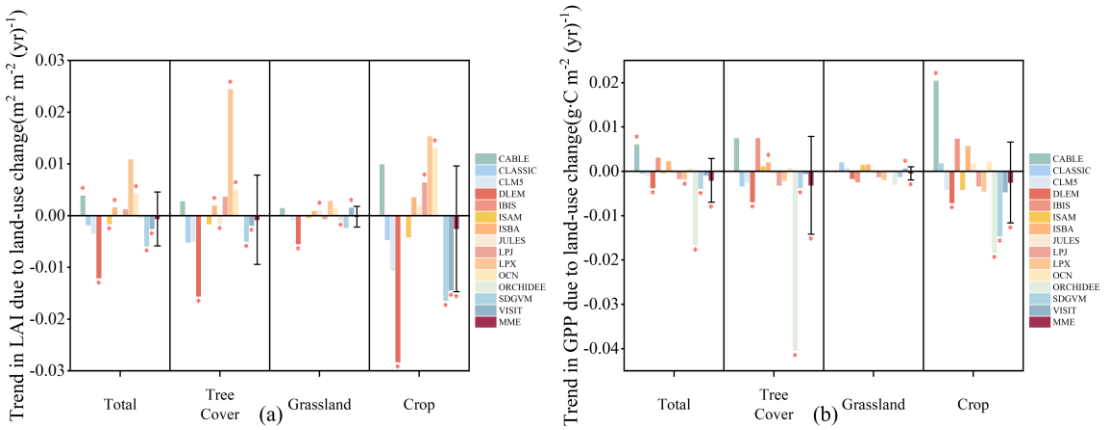

Figure S14. Impacts of land use change on (a) LAI, (b) GPP considered by the models (S3-S2 scenario). The asterisk (*) indicated the significant trend ($p<0.05$).

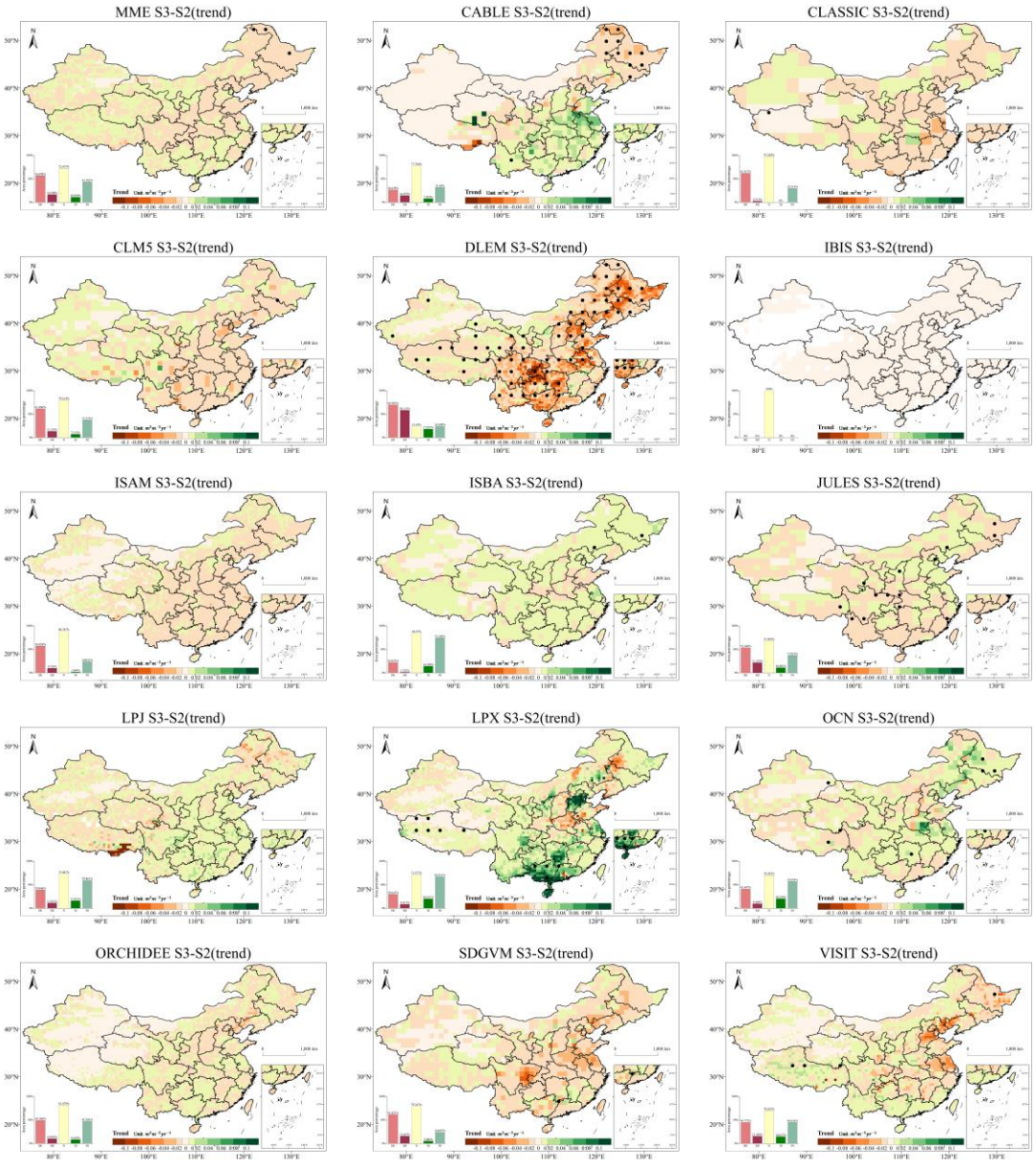

Figure S15. Interannual trends in changes in the impact of land use change on LAI considered by different models (S3-S2 scenario). Pink color represents the percentage of area of declining areas (DE), red color represents the percentage of area of significantly declining areas (SD), yellow color represents the percentage of area of areas with no significant change (N), green color represents the percentage of area of significantly increasing areas (SI), and light green color represents the percentage of area of increasing areas (IN). The dot indicated the significant trend ($p<0.05$).

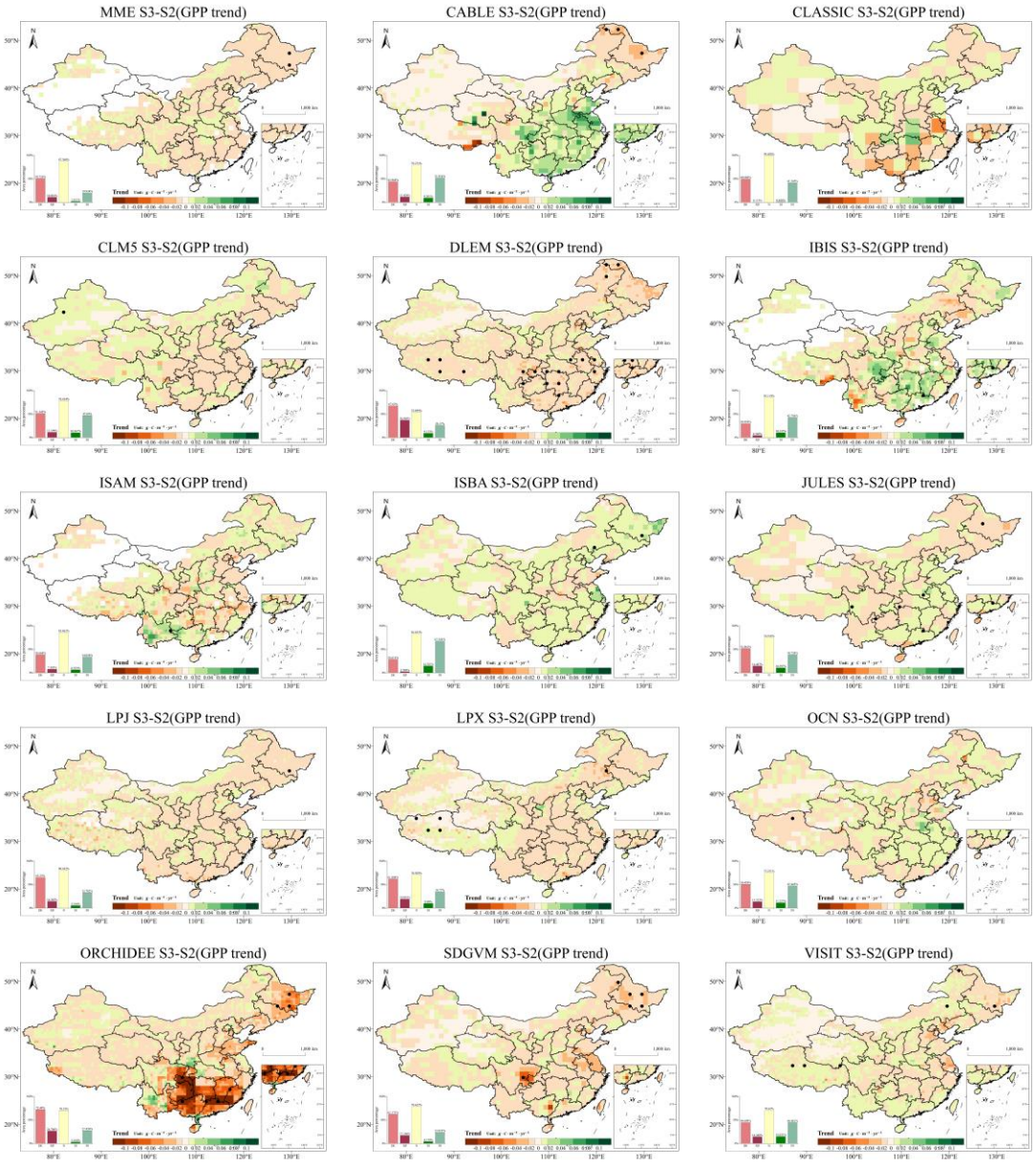

Figure S16. Interannual trends in changes in the impact of land use change on GPP considered by different models (S3-S2 scenario). Pink color represents the percentage of area of declining areas (DE), red color represents the percentage of area of significantly declining areas (SD), yellow color represents the percentage of area of areas with no significant change (N), green color represents the percentage of area of significantly increasing areas (SI), and light green color represents the percentage of area of increasing areas (IN). The dot indicated the significant trend ($p<0.05$).

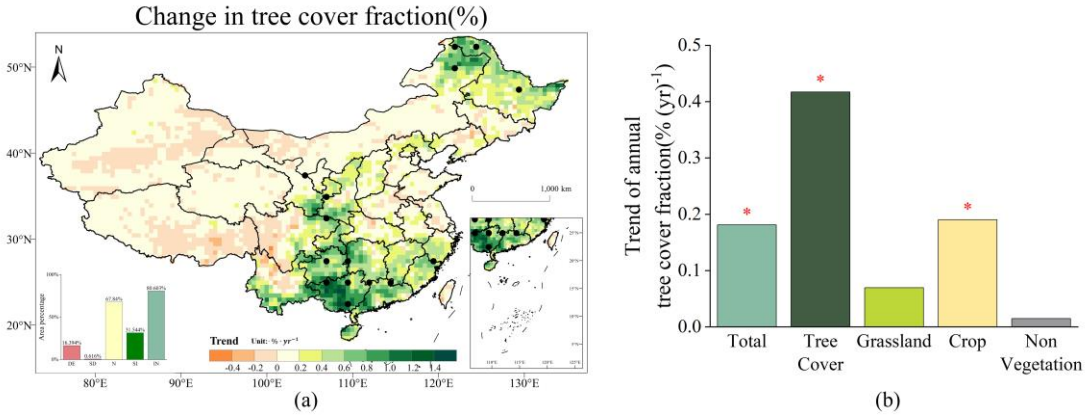

Figure S17. Changes in tree cover in China during 2003-2019. (a) The spatial tree cover changes in China. The dot indicated the significant trend ($p<0.05$). (b) The trend of overall annual mean tree cover fraction over different land use types. The asterisk (*) indicated the significant trend ($p<0.05$).

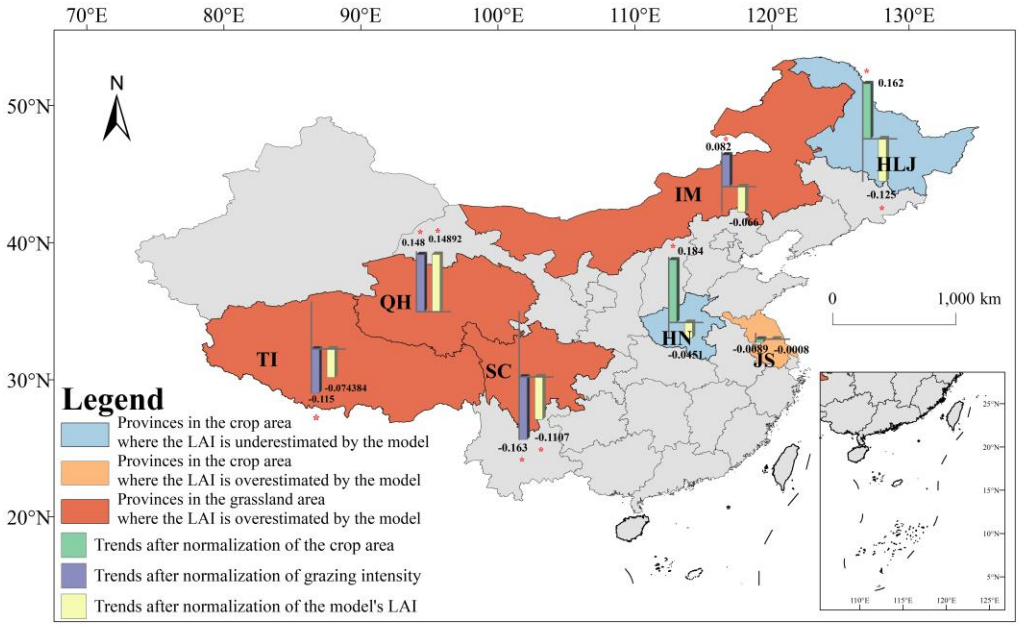

Figure S18. Comparison of standardized trends in grazing intensity versus crop acreage versus the effect of land use change on LAI trends considered by the model in China. In provinces dominated by grassland, the standardized trend of grazing intensity versus the simulated LAI S3-S2 scenario is compared; in provinces dominated by cropland, the standardized trend of crop acreage versus simulated LAI S3-S2 scenario is compared. Provinces in red and orange colors represent the overestimation of the trend of simulated LAI over the trend of observed LAI in the region; provinces in blue areas represent the underestimation of the trend of simulated LAI over the trend of observed LAI in the region. The asterisk (*) indicated the significant trend ($p<0.05$).

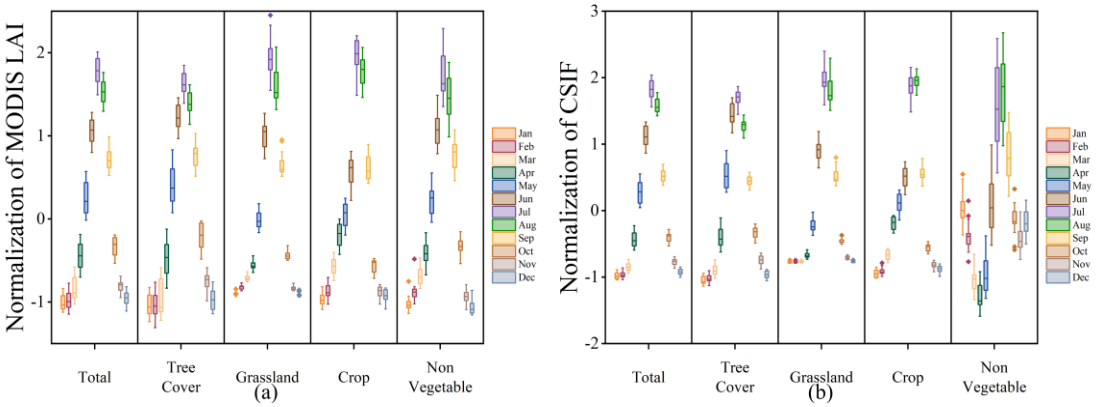

Figure S19. The normalized overall seasonal of observed data in China. (a) The MODIS LAI seasonal dynamics over different land use types; (b) The CSIF seasonal dynamics over different land use types.

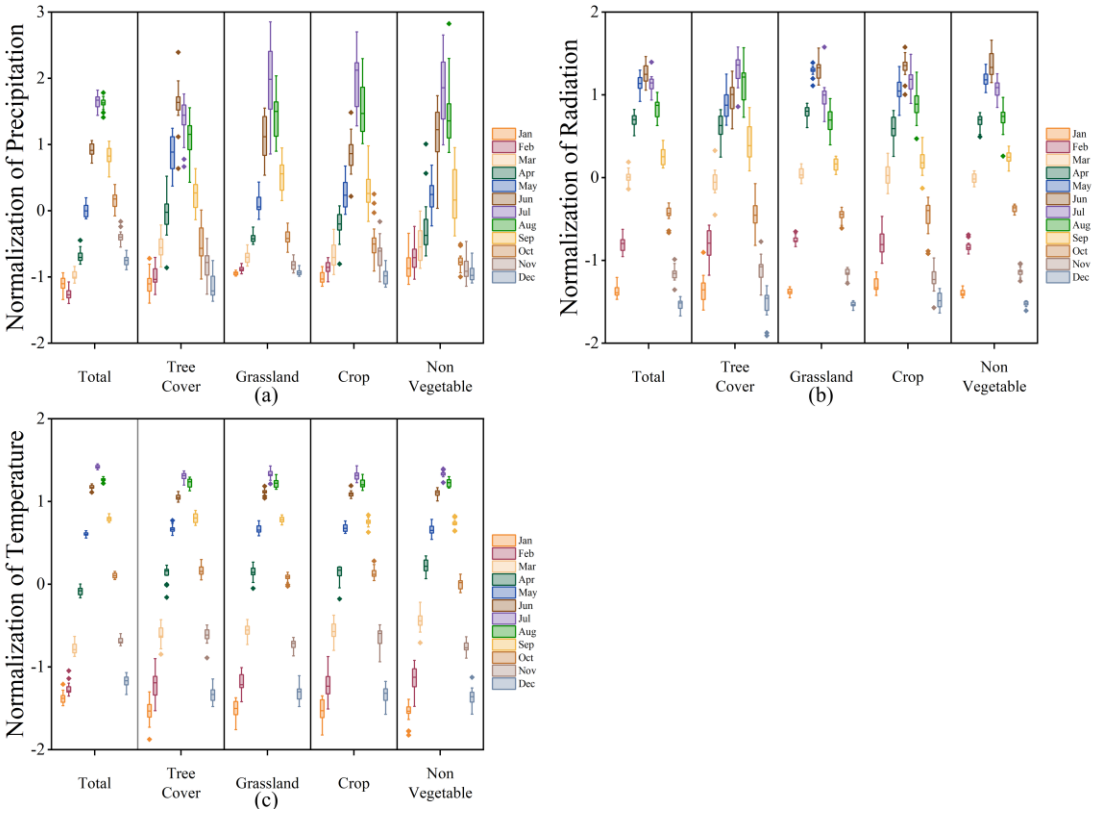

Figure S20. The normalized overall seasonal of precipitation, radiation and temperature in China. (a) The precipitation seasonal dynamics over different land use types. (b) The radiation seasonal dynamics over different land use types. (c) The temperature seasonal dynamics over different land use types.

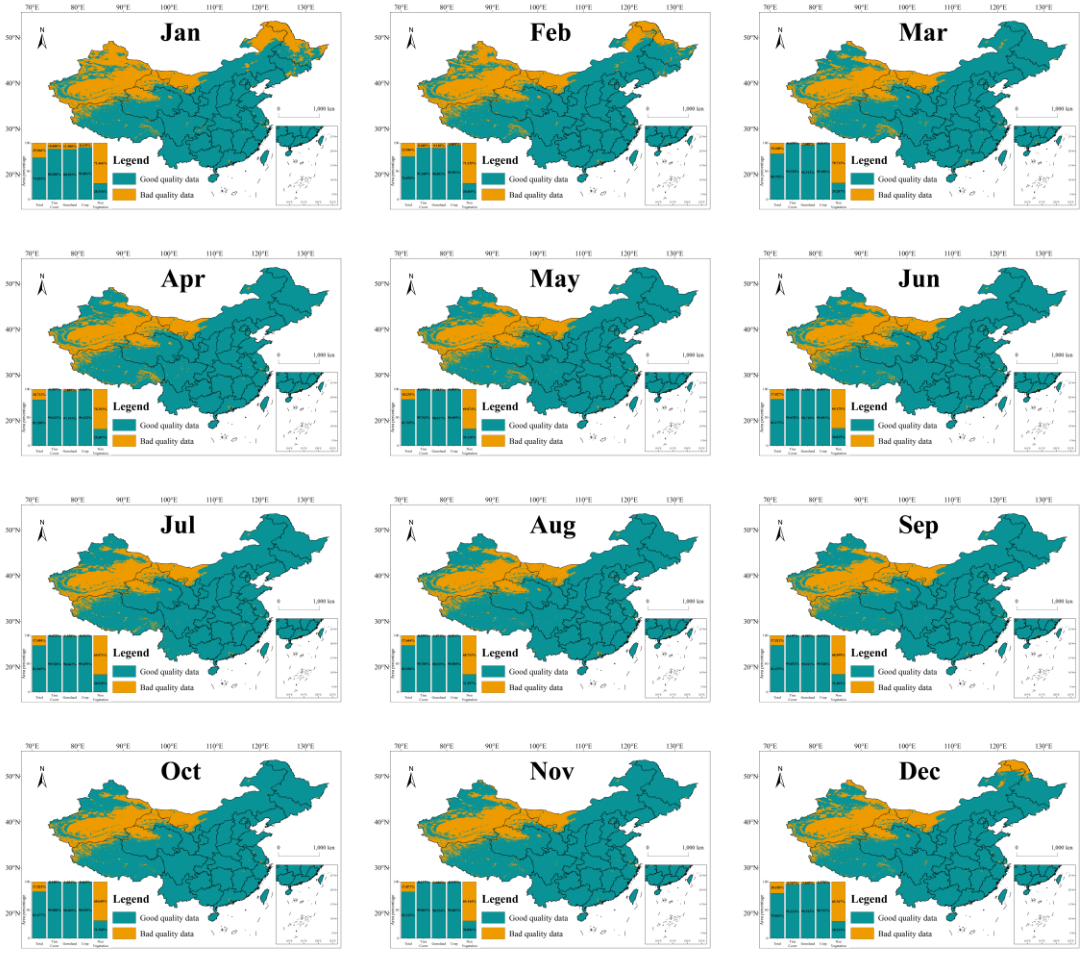

Figure S21. Spatial distribution of pixel quality and the percentage of area with high and low pixel quality in different months for the whole and for different land use types in China. Green color represents high quality pixels and yellow color represents low quality pixels.